

Quantifying Altitudinal Mercury Accumulation in Biomonitors along Himalayan Valleys Using Mercury Isotopes

Xinyuan Cai, Wei Yuan, Qiangong Zhang, Kang Luo, Yiyuan Xu, Ge Zhang, Fei Wu, Longyu Jia, Meiqing Sun, Nantao Liu, Che-Jen Lin, Xun Wang,* and Xinbin Feng



Cite This: *Environ. Sci. Technol.* 2024, 58, 22183–22193



Read Online

ACCESS |



Metrics & More



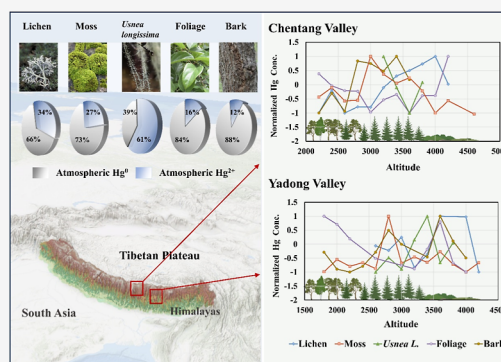
Article Recommendations



Supporting Information

ABSTRACT: The Himalayan valleys are important transport channels of atmospheric pollutants from South Asia to the Tibetan Plateau. This study aims to demonstrate the use of biomonitors (i.e., tree foliage, bark, mosses, and lichens) in the Himalayas to understand the sources and accumulation of mercury (Hg), including the transboundary atmospheric Hg transport across the Himalayas. Results showed that the significant variability in the physiological characteristics and nutrient uptake pathways, coupled with rapid changes in topography and climate-forced precipitation, led to significant differences in concentrations and isotopic compositions among biomonitor species. $\Delta^{199}\text{Hg}$ values (-0.32 to -0.10‰) at the lower altitudes were slightly more positive than values at upper altitudes, likely reflecting signals of transboundary transport of anthropogenic Hg from South Asia. The isotope mixing model determined atmospheric Hg^0 as the main source of Hg in most biomonitors ($67 \pm 13\%$ to $88 \pm 13\%$), except for *Usnea longissimas* (i.e., a unique type of lichen) with $61 \pm 16\%$ contribution of atmospheric Hg^{2+} . Additionally, the morphological structure and epiphytic environment of *U. longissimas* facilitate aqueous Hg secondary reactions. Our results suggest that the Hg cycling in the Himalayan valleys could mix multiple impacts from montane environments and signals of transboundary transport of anthropogenic Hg from South Asia.

KEYWORDS: mercury, deposition, isotopes, biomonitors, Himalayan valleys



1. INTRODUCTION

Mercury (Hg) is a global concern toxic pollutant. The long-distance transport of anthropogenic Hg and the subsequent deposition in regions of little anthropogenic release threaten the health of ecosystems and human.^{1–4} Known as the “Roof of the World”, the Qinghai-Tibet Plateau (QTP) has an average altitude of over 4000 m above sea level. Though far away from anthropogenic Hg emission sources,^{5,6} the QTP is confronted with a high level of Hg pollution risk.^{6,7} The Hg accumulation rate in lake sediments and ice cores of the QTP has increased by 2 to 7 times since the 1850s,^{8,9} suggesting distinct anthropogenic impacts on Hg deposition.

The Indian monsoon controls the transboundary atmospheric transport in the southern regions of the QTP.^{9–11} The convective storms induced by the Indian monsoon can transport anthropogenic Hg from South/Southeast Asia across the Himalayas, the highest mountain system in the world, via midtropospheric circulation.¹² The south-north longitudinal valleys in the Himalayas provide water channels.^{13,14} The upslope winds bring atmospheric pollutants through these valleys over the Himalayas.^{15–18} Observational evidence has been found for persistent organic pollutants (POPs). The POP transport flux induced by the valley wind is 2 to 3 times higher than the flux across the mountain ridges.¹⁹ This leads us to

hypothesize that the valleys across the Himalayas provide the transport pathway for atmospheric Hg because of the similar physiochemical properties of Hg and POPs. Yet, lack of data in Hg concentration, process details, and not identified Hg sources warrant the Hg observations along these valleys.

Direct measurement of atmospheric Hg in the Himalayas is challenging due to the harsh environments and lack of access and utilities. The continuous uptake of atmospheric Hg by vegetative biomasses (e.g., tree foliage, bark, moss, and lichen) could retain the transport signals where the vegetations serve as the biomonitors. Vegetative biomonitors have been utilized to monitor atmospheric Hg pollution levels with the advantages of easy collection and cost-effectiveness.^{20–25}

Generally, Hg in tree foliage, bark, moss and lichen mainly comes from uptake of atmospheric Hg, and to a lesser degree, Hg translocation by root uptake of soil Hg.^{2,26} Their sensitivities in reflecting atmospheric Hg pollution depend on individual

Received: September 25, 2024

Revised: November 25, 2024

Accepted: November 27, 2024

Published: December 4, 2024



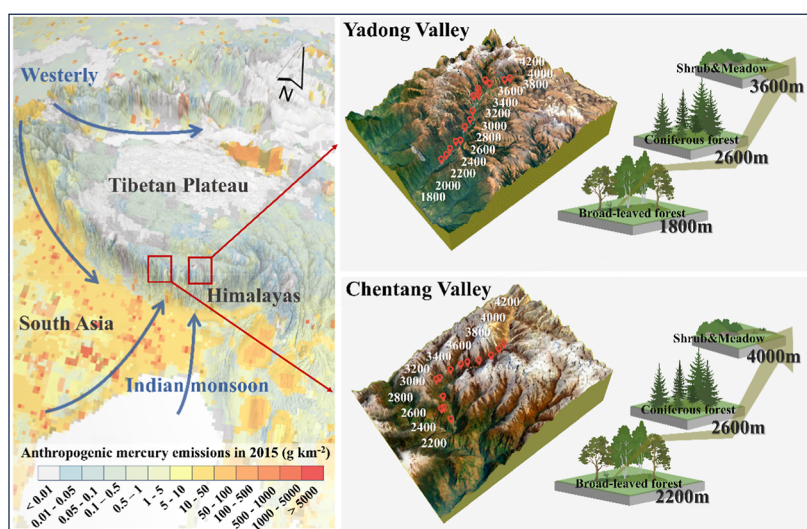


Figure 1. Sampling locations and vegetation distribution in selected two valleys in the Himalayas. The anthropogenic Hg emission data are obtained from AMAP/UNEP geospatially distributed 2015 Hg emission data set.

physiological and morphological characteristics. Vascular foliage primarily accumulates Hg through stomatal and cuticular uptake of atmospheric Hg^0 . The translocation of Hg from soils to above-ground tissues is less understood.^{27,28} Mercury in tree bark comes mainly from foliage translocation via phloem after uptake of atmospheric Hg^0 by foliage or from surface-absorption of atmospheric Hg (specifically particle-bound Hg^{2+}).^{2,26} Non-vascular vegetations, including lichens and mosses, accumulate Hg by absorbing diffused air Hg (both Hg^0 and Hg^{2+}) through its cell membranes.^{23,29,30} The plant's physiological and morphological characteristics would influence the accumulation rate of Hg accumulation species in biomonitors along the altitude of valley. Additionally, the elevation gradient in the Himalayan valleys is sharp, leading to a complicated montane climate and rapid changes in vegetation.^{18,31,32} These environmental factors can influence atmospheric Hg cycling in ecosystems. Thus, it is required to examine the representativeness of the biomonitor data in relation to the signals of Hg transport for assessing Hg transport, uptake, and deposition in the Himalayas.

Hg isotopic techniques are a powerful tool to trace Hg sources and their fate in the environment. Mercury has unique three-dimensional isotopic fractionations, which include mass-dependent fractionation (MDF, expressed as $\delta^{202}\text{Hg}$), odd mass-independent fractionation (odd-MIF, $\Delta^{199}\text{Hg}$ and $\Delta^{201}\text{Hg}$), and even mass-independent fractionation (even-MIF, $\Delta^{200}\text{Hg}$ and $\Delta^{204}\text{Hg}$).^{33–35} The atmospheric Hg^0 , atmospheric Hg^{2+} , and anthropogenic Hg all have unique Hg isotopic signatures.^{36–38} Odd-MIF only occurs in a few Hg biogeochemical processes, such as the photoreduction of Hg^{2+} .^{39,40} Even-MIF is associated with the oxidation of Hg^0 to Hg^{2+} in the upper atmosphere. There are known processes of Hg translocation and transformation at the interface of air-vegetation-soil that produce even-MIF, making $\Delta^{200}\text{Hg}$ as a superior tracer for atmospheric Hg^{2+} .^{34,41–47} Overall, the $\delta^{202}\text{Hg}$, $\Delta^{199}\text{Hg}$ and $\Delta^{200}\text{Hg}$ values of biomonitors are useful for determining their Hg sources and identifying the specific biogeochemical processes by analyzing shifts of Hg-MDF and -MIF signatures.

The objectives of this study are to (1) investigate the distribution of atmospheric Hg levels along the elevation of the

Himalayan valleys; (2) understand Hg sources and accumulation processes through stable Hg isotope signals in biomonitors; and (3) identify transboundary atmospheric Hg transport and internal Hg biogeochemical processes at the interface of air and biomonitors. We selected two valleys, the Yadong Valley and Chentang Valley, in the Himalayas and collected typical biomonitors. Then, we used Hg isotopes to trace Hg sources and accumulation processes in different biomonitors. Implications for atmospheric Hg cycling along valleys of the Himalayas were discussed.

2. METHODOLOGY

2.1. Site Description. Two typical valleys in the Himalayas are selected in this work, including the Yadong Valley and Chentang Valley (Figure 1). The Yadong Valley is located between $87^{\circ}21'–87^{\circ}26'$ E and $27^{\circ}13'–27^{\circ}54'$ N and borders India. It stretches from south to north, with an altitude variation over 4000 m. The Chentang Valley is located between $88^{\circ}48'–89^{\circ}03'$ E and $27^{\circ}23'–27^{\circ}48'$ N and borders Nepal, also with an altitude variation over 4000 m. At an altitude of 3200 m of the Chentang Valley, its direction shifts from south-north to west-east. There is a distinct montane climate controlled by the Indian monsoon for two valleys (Figure 1). The climate changes from maritime humid weather in the lower elevation to continental arid weather in the upper elevation. The terrain is flat and wide in the low-altitude regions (1800–2800 m), with subtropical evergreen-deciduous broadleaf mixed forests. The detailed plant types along with elevation can be found in the Supporting Information.

2.2. Sample Collection and Pretreatment. The biomonitors in this study include tree foliage, tree bark, moss, and lichen. The sampling sites in the Yadong Valley ranged from an elevation of 1800 to 4200 m with an interval of 200 m between adjacent two sites and in the Chentang Valley ranged from 2200 to 4600 m. Each sampling site was at least 200 m from the roadway to avoid the direct anthropogenic impacts. To attain statistical significance, we collected three replicate samples for each biomonitor at each site. Notably, *Usnea longissima* was investigated separately in this study due to its unique morphological characteristics and epiphytic habitat across different altitudes, distinguishing it from other common lichens.

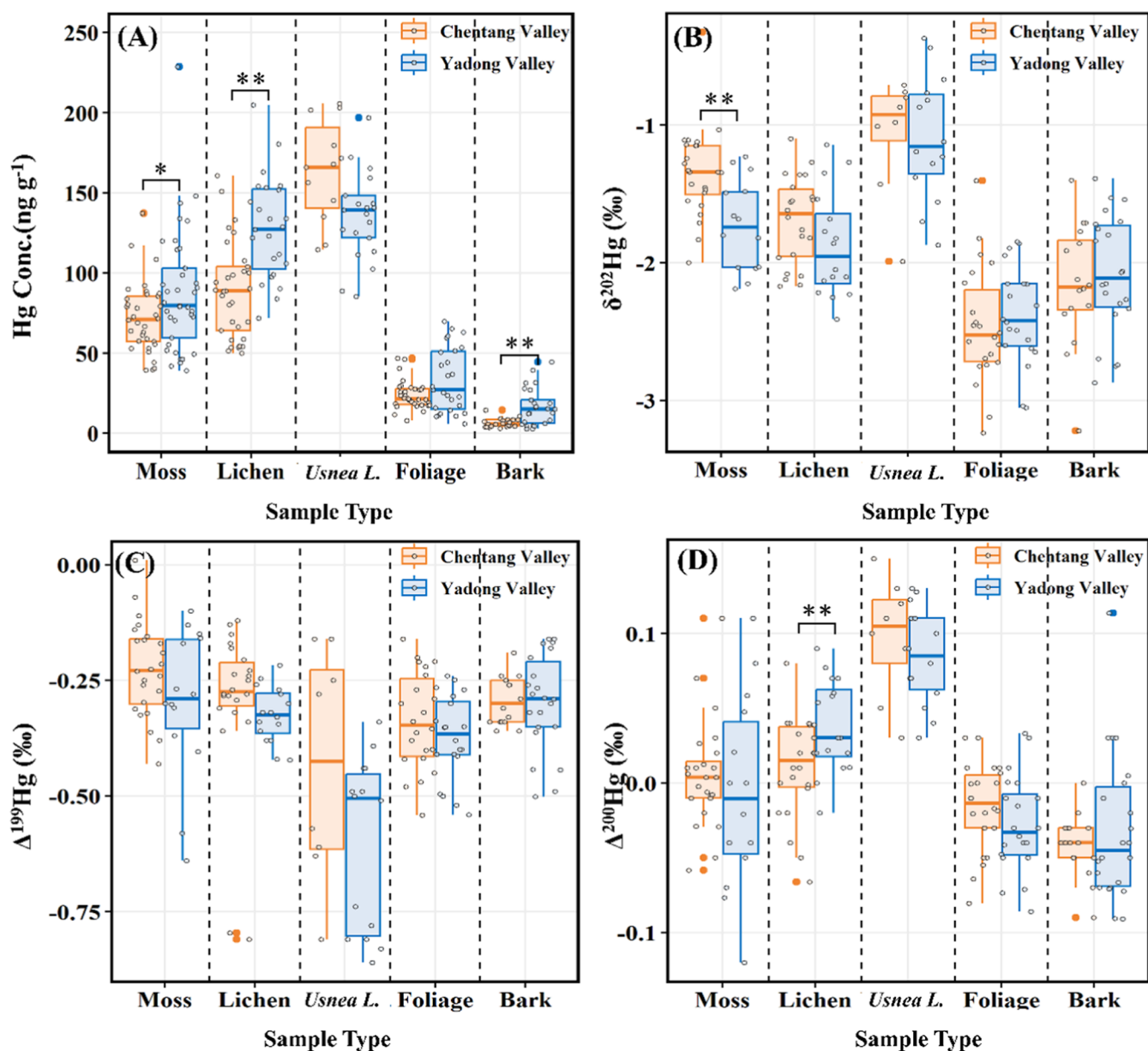


Figure 2. Comparisons of (A) Hg concentration, (B) $\delta^{202}\text{Hg}$ values, (C) $\Delta^{199}\text{Hg}$ values, and (D) $\Delta^{200}\text{Hg}$ values among moss, lichen, *Usnea longissima*, foliage and bark in the Chentang Valley and Yadong Valley. The asterisk (*) represents a statistical difference at the 95% confidence level.

Hereafter, the lichen mentioned in this study did not contain the species of *U. longissima*. Our sampled mosses and lichens grow on stem bark below the elevation of 4000 m, and grow on stones above 4000 m. We did not sample the mosses growing on the ground to avoid the impacts from the soil. Overall, we collected 284 biomonitor samples in August of 2022, including 73 mosses, 55 lichens, 33 *U. longissimas*, 70 tree foliage, and 53 tree barks (Figure 1).

After collection, all samples were lightly washed with ultrapure water to remove surface dust and soil in the laboratory. After the water was drained, all samples were placed in an oven at 40 °C and dried to a constant weight. Our earlier studies have documented that oven-drying at 40 °C would not lead to a significant Hg mass loss in vegetation.^{48,49} After drying, all samples were ground into a fine powder using a grinder and stored in sealable polyethylene bags. The grinding tools were wiped clean with ethanol before grinding the next sample to prevent cross-contamination.

2.3. Hg Concentration and Isotope Measurements. Hg concentrations in samples were measured by using a DMA-80 Hg analyzer. We determined Hg concentrations of one certified plant reference material and one parallel sample in every nine samples. The average recovery of certified plant reference material (NIST SRM 1515, Hg concentration: $44.0 \pm 2.2 \text{ ng g}^{-1}$) was $100.7 \pm 4.5\%$ ($n = 35$). The bias of the parallel sample was less than 5%.

Preconcentration of Hg in plant samples and determination of Hg isotopic compositions have been described in our earlier studies.^{50–52} We selected two samples of every biomonitor at each sampling site to measure the Hg isotopic compositions. The selected samples were processed by double-stage heating pyrolysis in a tube muffle furnace. The Hg vapor evaded from the sample was then captured by using 5 mL of 40% reverse aqua regia ($\text{HCl}/\text{HNO}_3 = 1:3, \text{ v/v}$) trapping solution. The Hg concentration enriched in the trapping solution was measured by cold vapor atomic fluorescence spectrometry (Tekran 2500)

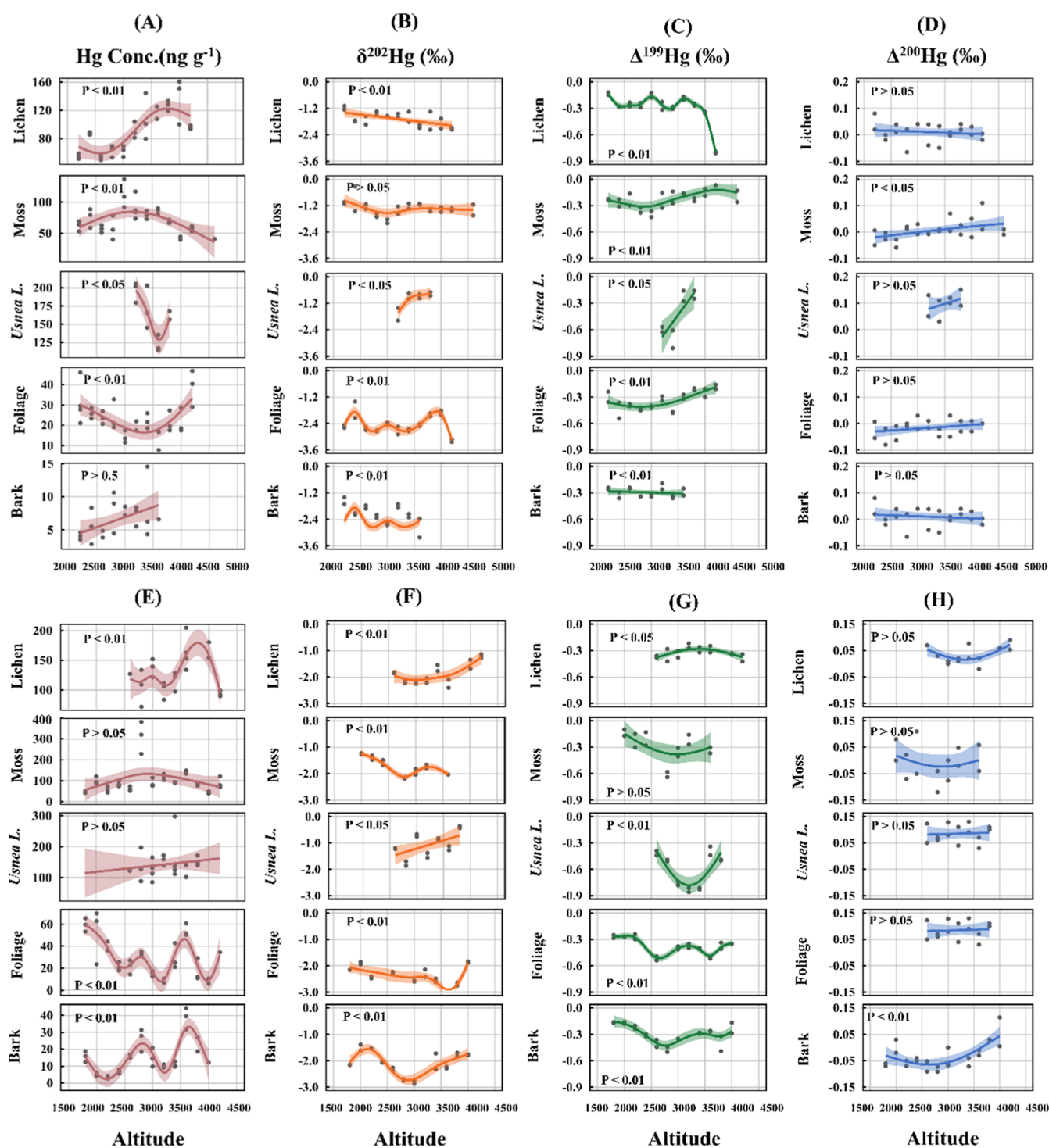


Figure 3. Altitudinal trends of Hg concentrations and Hg isotope signatures by using Generalized Additive Models (GAMs). (A) Hg concentration in the Chentang Valley, (B) $\delta^{202}\text{Hg}$ values in the Chentang Valley, (C) $\Delta^{199}\text{Hg}$ values in the Chentang Valley, (D) $\Delta^{200}\text{Hg}$ values in the Chentang Valley, (E) Hg concentration in the Yadong Valley, (F) $\delta^{202}\text{Hg}$ values in the Yadong Valley, (G) $\Delta^{199}\text{Hg}$ values in the Yadong Valley, and (H) $\Delta^{200}\text{Hg}$ values in the Yadong Valley. We added error bounds to illustrate the uncertainty of the fitted trends in (A–H).

following US-EPA method 1631. The preconcentration recovery of certified plant reference material was $99.8 \pm 5.3\%$ (BCR-482, $n = 9$). The preconcentration recovery of samples was $96.7 \pm 11.3\%$ ($n = 178$). The Hg isotopic compositions were determined by a multicollector inductively coupled plasma mass spectrometer (MC-ICP-MS, Neptune Plus, Thermo Scientific). The trapping solution was diluted to 0.5 ng mL^{-1} and imported into the gas–liquid separator with 3% SnCl_2 solution.

The Hg-MDF is reported in δ notation using the unit of permil (‰) referenced to the neighboring NIST-3133 solution

$$\delta^{202}\text{Hg} (\text{‰}) = 1000 \times \left[\frac{(^{202}\text{Hg}/^{198}\text{Hg})_{\text{sample}}}{(^{202}\text{Hg}/^{198}\text{Hg})_{\text{NIST-3133}}} - 1 \right] \quad (1)$$

The MIF is reported as $\Delta^{xxx}\text{Hg}$ following the convention proposed by Blum and Bergquist⁵³

$$\Delta^{199}\text{Hg} (\text{‰}) = \delta^{199}\text{Hg} - 0.2520 \times \delta^{202}\text{Hg} \quad (2)$$

$$\Delta^{200}\text{Hg} (\text{‰}) = \delta^{200}\text{Hg} - 0.5024 \times \delta^{202}\text{Hg} \quad (3)$$

$$\Delta^{201}\text{Hg} (\text{‰}) = \delta^{201}\text{Hg} - 0.7520 \times \delta^{202}\text{Hg} \quad (4)$$

To evaluate whether isotopic composition bias occurred during the preconcentration, we determined the Hg isotopic compositions of certified plant reference material BCR-482. Results of BCR-482 were $\delta^{202}\text{Hg} = -1.44 \pm 0.10\text{‰}$, $\Delta^{199}\text{Hg} = -0.63 \pm 0.10\text{‰}$, $\Delta^{201}\text{Hg} = -0.64 \pm 0.09\text{‰}$, $\Delta^{200}\text{Hg} = 0.07 \pm 0.04\text{‰}$ (mean $\pm 2\sigma$, $n = 9$, Table S3). The NIST-8610 standard solution was also measured in every 10 to 15 samples as the secondary standard with results of $\delta^{202}\text{Hg} = -0.52 \pm 0.07\text{‰}$, $\Delta^{199}\text{Hg} = 0.01 \pm 0.10\text{‰}$, $\Delta^{201}\text{Hg} = 0.00 \pm 0.09\text{‰}$, and $\Delta^{200}\text{Hg} = 0.00 \pm 0.06\text{‰}$ (mean $\pm 2\sigma$, $n = 16$, Table S3). These measured values were consistent with the reported results,^{53,54} thus indicating negligible isotopic bias during the preconcentration.

2.4. Hg Isotope Mixing Model. Two source endmembers for Hg accumulation in biomonitors were proposed: atmospheric Hg^0 and atmospheric Hg^{2+} inputs. Since known Hg biogeochemical processes in plants do not lead to an even-MIF, $\Delta^{200}\text{Hg}$ is a superior tracer to trace atmospheric Hg^{2+} . Therefore, we used a $\Delta^{200}\text{Hg}$ binary mixing model to estimate the contribution of atmospheric Hg^0 and atmospheric Hg^{2+} inputs

$$\begin{aligned} \Delta^{200}\text{Hg}_{\text{Hg}(0)} \times f_{\text{Hg}(0)} + \Delta^{200}\text{Hg}_{\text{Hg}(\text{II})} \times f_{\text{Hg}(\text{II})} \\ = \Delta^{200}\text{Hg}_{\text{plant}} \end{aligned} \quad (5)$$

where $\Delta^{200}\text{Hg}_{\text{Hg}(0)}$ is the signature of atmospheric Hg^0 inputs in the QTP and obtained from earlier observations ($-0.06 \pm 0.04\text{‰}$),¹² and $f_{\text{Hg}(0)}$ is the atmospheric Hg^0 input contribution. $\Delta^{200}\text{Hg}_{\text{Hg}(\text{II})}$ is the signature of atmospheric Hg^{2+} inputs ($0.20 \pm 0.04\text{‰}$),^{2,26,50} and $f_{\text{Hg}(\text{II})}$ is the atmospheric Hg^{2+} input contribution (Figure S1). The small SD range of $\Delta^{200}\text{Hg}_{\text{Hg}(\text{II})}$ is because of the remote location of the QTP sites, which has little direct influence by anthropogenic emissions.^{12,50} We used the Monte Carlo simulation to quantify uncertainties of the Hg isotopic mixing model (in more detail in Supporting Information). These uncertainties are quantified by generating one million groups of $\Delta^{200}\text{Hg}$ signatures randomly ranging from mean $-$ SD to mean $+$ SD to solve eq 5.

2.5. Statistical Analysis. Statistical analyses were conducted using IBM SPSS Statistics v25.0 and RStudio at a confidence level of 95%. When data were normally distributed, one-way ANOVA, paired samples t -test, and posthoc Tukey HSD tests were applied to assess differences of significance; otherwise, the Kruskal–Wallis test and Dunn's posthoc test were applied. Pearson correlation analysis was utilized to assess relationships among different variables. For data fitting, local polynomial regression and Generalized Additive Models (GAMs) were used. More details can be found in the Supporting Information.

3. RESULTS

3.1. Hg Concentrations and Isotopic Compositions.

Figure 2A and Table S1 depict the variation of Hg concentrations among different biomonitors. The *U. longissimas* had the highest average concentration (mean \pm SD, 150 ± 41 ng

g^{-1} , $n = 33$), followed by other lichens (106 ± 37 ng g^{-1} , $n = 55$) and mosses (88 ± 55 ng g^{-1} , $n = 73$), and the lowest in foliage (27 ± 15 ng g^{-1} , $n = 70$) and bark (12 ± 10 ng g^{-1} , $n = 53$). The Hg concentrations in mosses, lichens and bark in the Yadong Valley were 30–150% higher than those in the Chentang Valley (t -test, $p < 0.05$ for moss; $p < 0.01$ for bark and lichen), and the concentrations in *U. longissimas* and foliage between two valleys were insignificant (t -test, $p > 0.05$).

Figure 2B–D and Table S2 display Hg isotopic signatures in two valleys. The *U. longissimas* had an average $\delta^{202}\text{Hg}$ value of $-1.08 \pm 0.44\text{‰}$. Mosses and lichens had comparable values of $\delta^{202}\text{Hg}$ ($-1.48 \pm 0.38\text{‰}$ versus $-1.77 \pm 0.38\text{‰}$, $p > 0.05$ by the t -test). Foliage and bark had the largest negative $\delta^{202}\text{Hg}$ signatures with the value of $-2.42 \pm 0.39\text{‰}$ and $-2.11 \pm 0.43\text{‰}$, respectively ($p < 0.01$, Dunn's posthoc test). *U. longissimas* had the highest negative $\Delta^{199}\text{Hg}$ values ($-0.54 \pm 0.22\text{‰}$, $p < 0.01$). There were insignificant differences in $\Delta^{199}\text{Hg}$ values among mosses (mean = $-0.25 \pm 0.13\text{‰}$), lichens (mean = $-0.31 \pm 0.14\text{‰}$), foliage (mean = $-0.36 \pm 0.10\text{‰}$) and bark (mean = $-0.30 \pm 0.09\text{‰}$). *U. longissimas* had the highest positive $\Delta^{200}\text{Hg}$ values (mean = $0.09 \pm 0.04\text{‰}$), followed by lichens (mean = $0.02 \pm 0.04\text{‰}$), mosses (mean = $0.00 \pm 0.05\text{‰}$), foliage (mean = $-0.02 \pm 0.03\text{‰}$) and bark (mean = $-0.04 \pm 0.04\text{‰}$).

The isotopic signals in the foliage and bark showed insignificant differences between the two valleys. The mean moss $\delta^{202}\text{Hg}$ value of Chentang Valley was significantly higher than the value of Yadong Valley ($-1.34 \pm 0.33\text{‰}$ versus $-1.73 \pm 0.33\text{‰}$, $p < 0.01$ by t -test), and $\Delta^{200}\text{Hg}$ in lichen of Yadong Valley was $0.03 \pm 0.03\text{‰}$ and in Chentang Valley was $0.01 \pm 0.03\text{‰}$. There were insignificant correlations among Hg concentrations, $\delta^{202}\text{Hg}$, $\Delta^{199}\text{Hg}$ and $\Delta^{200}\text{Hg}$ in biomonitors (Figures S2 and S3).

3.2. Altitudinal Distributions. The Hg concentration in lichens increased with increasing altitude of the Chentang Valley (Figure 3A). The other biomonitors in the Chentang Valley did not show consistent altitudinal gradients. The *U. longissimas* had the lowest Hg concentration (122 ± 11 ng g^{-1}) at 3600 m altitude in the Chentang Valley, and mosses had the highest Hg concentration (113 ± 23 ng g^{-1}) at 3000 m altitude. The Hg concentrations in all biomonitors of Yadong Valley varied largely from the elevation of 2500 to 4000 m (Figure 3E). The Hg concentrations in lichens, foliage and bark reached their peaks at 3600 m altitude in the Yadong Valley. Moss Hg concentrations in the Yadong Valley were highest (311 ± 77 ng g^{-1}) at an altitude of 2800 m.

As shown in Figure 3B–D, Hg isotopic signatures in the biomonitors of Chentang Valley did not vary significantly along with altitude (ANOVA test, $p > 0.05$). However, *U. longissimas* had more negatively isotopic values at mid-altitude (3000–3500 m). There were distinct fluctuations in $\delta^{202}\text{Hg}$ and $\Delta^{199}\text{Hg}$ signatures of mosses, *U. longissimas*, foliage and bark along the altitude of Yadong Valley (Figure 3F–H). Notably, *U. longissima* $\Delta^{199}\text{Hg}$ values were distinctly negative ($-0.80 \pm 0.04\text{‰}$) at 3000–3500 m altitudes in the Yadong Valley. Moss $\Delta^{199}\text{Hg}$ values in the Yadong Valley were most negative ($-0.61 \pm 0.04\text{‰}$) at an altitude of 2800 m. Lichen $\Delta^{200}\text{Hg}$ signatures in the Yadong Valley and Chentang Valley did not have significant fluctuations along with the altitude (ANOVA test, $p > 0.05$).

4. DISCUSSION

4.1. Hg Accumulation in Biomonitors. Mercury in tree bark derives from foliage translocation via tree phloem after

uptake of atmospheric Hg⁰ by foliage or from direct absorption of atmospheric Hg (specifically particle-bound Hg) by its porous surface.^{23,55–57} In the studied region, Hg in the bark originates mainly from foliage translocation. This is supported by several observations. First, the average Hg concentrations in the bark of both valleys were ~50% of values in foliage (*t*-test, *P* < 0.01), consistent with the Hg translocation gradient from foliage to bark.²⁶ The $\Delta^{199}\text{Hg}$ and $\Delta^{200}\text{Hg}$ serve as useful tracers to identify Hg sources in bark since little Hg-MIF occurs during the translocation process. Our results showed comparable $\Delta^{199}\text{Hg}$ and $\Delta^{200}\text{Hg}$ values between bark and foliage (*t*-test, *P* > 0.05), suggesting similar Hg sources. In addition, the $\delta^{202}\text{Hg}$ values in bark showed a positive shift of only 0.3‰ compared to those of foliage, but a negative shift up to -3.2‰ compared to signatures of atmospheric total Hg in the QTP.¹² There is a small MDF occurring during the direct Hg absorption by bark lenticels but up to -2.8‰ to -2.6‰ shift of $\delta^{202}\text{Hg}$ during the uptake of atmospheric Hg⁰ by foliage stomata.^{26,37} This confirms that Hg in the bark mainly comes from foliage translocation.

There were insignificant differences in Hg concentrations and isotopic signals between mosses and lichens in the Yadong Valley (*t*-test, *p* > 0.05). However, the Hg concentration in lichens of Chentang Valley was 25% higher than that in mosses (*t*-test, *p* < 0.05), and the $\delta^{202}\text{Hg}$ value in lichens was 0.35‰ lower than the value in mosses (*t*-test, *p* < 0.01). The differences in topography and climate in Chentang and Yadong likely contribute to the distinct Hg concentrations and isotopic signals between moss and lichen. The shifts of valley direction at the mid-elevation of Chentang Valley (i.e., from south-north to west-east) change the local hydrothermal conditions and water transport within the valley. The differences between moss and lichen in adapting to climatic changes would affect the Hg uptake by the two plant types, leading to the faster reactions of lighter isotopes in mosses.^{20,23,58}

Hg concentrations in mosses and lichens were 2–10 times of Hg concentrations in foliage in both valleys at the same altitude. The $\Delta^{200}\text{Hg}$ signals in mosses and lichens were significantly higher than those in foliage at the same altitude ($\sim 0.09\text{‰}$ shift). Since $\Delta^{200}\text{Hg}$ is a superior tracer for atmospheric Hg²⁺,^{33,41,59,60} the greater positive $\Delta^{200}\text{Hg}$ values in mosses and lichens suggest Hg sources from atmospheric Hg²⁺. This is related to the physiological characteristics and epiphytic environment of mosses and lichens. Due to the lack of a thick waxy cuticle layer, mosses and lichens obtain water and nutrients through the entire plant, thus making it more efficient in capturing atmospheric Hg wet deposition than vascular foliage.^{20,57,61,62} Additionally, the $\delta^{202}\text{Hg}$ signals in mosses and lichens were more positive than those in foliage (*t*-test, *p* < 0.01). This can be explained by the distinct pathways of atmospheric Hg uptake. Mosses and lichens mainly absorb atmospheric Hg (including Hg⁰ and Hg²⁺) through diffusion.^{23,29,30,57} The incorporation of atmospheric Hg to extracellular or intracellular exchange sites in moss and lichen is a rapid and passive physicochemical process.^{20,63,64} However, foliage primarily absorbs atmospheric Hg⁰ through stomata, influenced mainly by vegetation physiology.^{26,57} The complicated and physiology-controlled process would lead to a greater shift in $\delta^{202}\text{Hg}$ during foliage uptake of air Hg⁰.^{26,37,51,65}

Notably, *U. longissima* showed the highest $\Delta^{200}\text{Hg}$ signals (Figure 2D). This indicates the elevated atmospheric Hg²⁺ sources in *U. longissimas*. The elevated atmospheric Hg²⁺ sources in *U. longissima* can be attributed to its unique morphological structure and epiphytic environment. *U. long-*

issima features a central cord-like structure (cord axis) surrounded by multilayered symbiotic tissues, which provide a large specific surface area, enhancing water absorption efficiency compared to general leafy and crustaceous lichens.^{66,67} Additionally, *U. longissima* hangs from branches and has higher chances to obtain montane fogwater than other lichens attaching on tree trunks.

4.2. Factors Affecting Altitudinal Distribution. The Hg concentration and isotopic signatures in biomonitors are without consistent altitudinal gradients in Figure 3. This is because of the interplays of climate, topography, and vegetation forcing a complicated Hg cycling in the Himalayan valleys. We discussed these combined impacts as follows.

The climate, specifically the forced changes of precipitation type (i.e., rainfall and cloudwater) and amount along the altitude, can influence Hg transformation (e.g., redox reactions) and Hg accumulation in biomonitors. Hg concentrations in lichens peaked at 3600 m altitude in the Yadong Valley. Similarly, the Hg concentrations of lichens and mosses at mid-altitude (2800–3800 m) of Chentang Valley reached 1.5 times those in the lower region (*t*-test, *p* < 0.01). The trend of cloudwater likely plays an important role in shaping the altitudinal distribution of Hg concentrations because the higher cloudwater quantity at mid-altitude significantly increased wet deposition of atmospheric Hg.^{60,68–71}

Altitudinal changes in vegetation species and types, which are controlled by the montane climate, also affect Hg accumulation in biomonitors at different altitudes. The tree species shift from evergreen broadleaf species at low elevations to deciduous and coniferous species at high elevations. Similarly, lichen shifts from fruticose and foliose to crustose species.^{7,69,72,73} This could lead to large heterogeneities in the Hg concentration among various altitudes. We found that the Hg concentration of broadleaf foliage in the Yadong Valley was about twice that of coniferous foliage (40 ± 21 versus 22 ± 14 ng g⁻¹, *p* < 0.01), while little difference was observed in the Chengtang Valley (*t*-test, *P* > 0.05). This is caused by the combined effect of leaf morphology and foliage lifespan on atmospheric Hg uptake. Broadleaf foliage has a larger leaf area and a higher stomatal density, both favor Hg accumulation. In contrast, coniferous foliage has a longer lifespan (1–5 years) than broadleaf foliage (1–3 years), and the longer lifespan increases the quantity of atmospheric Hg uptake.^{74–77} Variation of forest canopy structure (e.g., canopy height, canopy cover, and canopy roughness) along the elevation also significantly affect atmospheric Hg⁰ and Hg²⁺ depositions.^{69,71,72} These factors collectively led to observed Hg accumulation in biomonitors.

At 1800–2400 m altitude in the Yadong Valley, $\Delta^{199}\text{Hg}$ values were from -0.32 to -0.10‰ , slightly more positive than values at upper altitudes (Figure 3G). These $\Delta^{199}\text{Hg}$ values reflect anthropogenic Hg emission from South Asia. Anthropogenic Hg is associated with nearly to zero signals of $\Delta^{199}\text{Hg}$.^{36–38} Anthropogenic Hg emissions in South Asia amount to 240 Mg yr⁻¹ (Figure 1), approximately 10% of global anthropogenic Hg emissions.^{8,9} The Himalayan valley is the important trans-boundary transportation channel of other atmospheric pollutants (e.g., POPs), thus likely a case for Hg in low elevation regions.^{19,75,78} During the transport, the Hg biogeochemical processes mediated by topography, climate and vegetation could dilute the anthropogenic Hg signals in biomonitors,^{35,51} leading to more negative $\Delta^{199}\text{Hg}$ values at elevated sites. Additionally, the topography-induced variations of planetary boundary layer

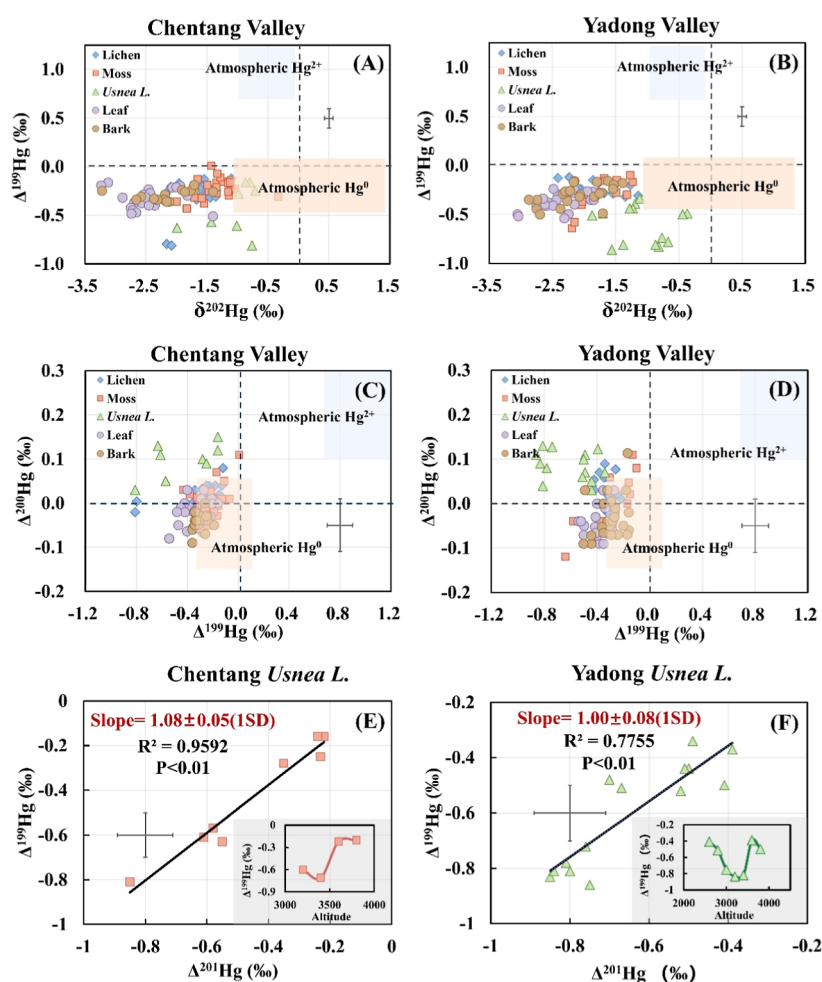


Figure 4. Hg isotopic signature and correlation. (A) $\Delta^{199}\text{Hg}$ versus $\delta^{202}\text{Hg}$ in biomonitors of Chentang Valley, (B) $\Delta^{199}\text{Hg}$ versus $\delta^{202}\text{Hg}$ in biomonitors of Yadong Valley; (C) $\Delta^{200}\text{Hg}$ versus $\Delta^{199}\text{Hg}$ in biomonitors of Chentang Valley, (D) $\Delta^{200}\text{Hg}$ versus $\Delta^{199}\text{Hg}$ in biomonitors of Yadong Valley; (E) $\Delta^{201}\text{Hg}$ versus $\Delta^{199}\text{Hg}$ in moss of Yadong Valley, and (F) $\Delta^{201}\text{Hg}$ versus $\Delta^{199}\text{Hg}$ in *U. longissimas* of Yadong Valley. The error bar represents ± 2 standard deviation.

would significantly influence the biomonitors' Hg isotopic compositions along with the elevation.^{79,80}

4.3. Source Attribution by the Hg Isotopic Model.

Earlier studies showed that geogenic Hg (i.e., Hg release from rock weathering) does not translocate from the tree root zone to foliage, and that moss and lichen almost do not absorb soil Hg because of a lack of root structure.^{26,57,81} Therefore, the contribution of geogenic sources to Hg accumulation in biomonitors is quite minimal. Since $\Delta^{200}\text{Hg}$ is a superior tracer for atmospheric Hg^{2+} ,^{33,35,41,59} its signals were utilized for estimating the relative contribution of atmospheric Hg^0 and Hg^{2+} inputs.

The modeling results showed that atmospheric Hg^0 was the main Hg source in bark and foliage, with the contributions of $88 \pm 13\%$ and $84 \pm 11\%$, respectively. Atmospheric Hg^0 contributed $73 \pm 17\%$ of Hg sources in mosses and $67 \pm 13\%$ in lichens except for *U. longissimas* (Figures S4 and 5A,B). Atmospheric Hg^{2+} was the main Hg source in *U. longissimas*, with $61 \pm 16\%$ contribution. This is consistent with the physiological traits and epiphytic environment of *U. longissimas* that adsorbs a greater amount of atmospheric Hg^{2+} .^{20,23,30,82}

The atmospheric Hg^0 contribution in the foliage and bark did not vary significantly along with the altitude in the two valleys (Figure S5). There was also a weak altitudinal trend of

atmospheric Hg^{2+} contribution in the Chentang Valley (Figure 5C), which can be explained by its specific topography. The prevailing valley direction of the Chentang Valley is from south to north at lower altitude but from west to east at higher altitudes. The changed valley orientation alters the local hydrothermal conditions and water transport within the valley, and subsequently influences atmospheric Hg^{2+} deposition along the altitude.^{5,7} Interestingly, the contribution of atmospheric Hg^{2+} of lichens and mosses in the Yadong Valley distinctly increased from 30% to 50% at 3000–4000 m (Figure 5D). This is because of the higher precipitation and the greater cloudwater amount at altitudes of 3000–4000 m, both increase Hg^{2+} deposition.^{60,69,83}

4.4. Postdepositional Processes in *U. longissima*. The Hg isotopic model has shown the atmospheric Hg^{2+} input being the main Hg source in *U. longissimas*. Using the $\Delta^{199}\text{Hg}$ data of atmospheric Hg^0 and Hg^{2+} in the QTP,^{12,50} the Hg isotopic mixing model estimates an average of $0.48 \pm 0.18\%$ for *U. longissimas* (Figure S6). However, *U. longissimas* did not exhibit positive $\Delta^{199}\text{Hg}$ values of atmospheric Hg^{2+} . Specifically, *U. longissimas* at mid-elevation sites of the Chentang Valley (3200–3400 m) and Yadong Valley (3000–3400 m) both showed unusual negative $\Delta^{199}\text{Hg}$ values, up to -0.86% (Figure 4E,F). Earlier studies suggest that Hg^0 re-emission from plants

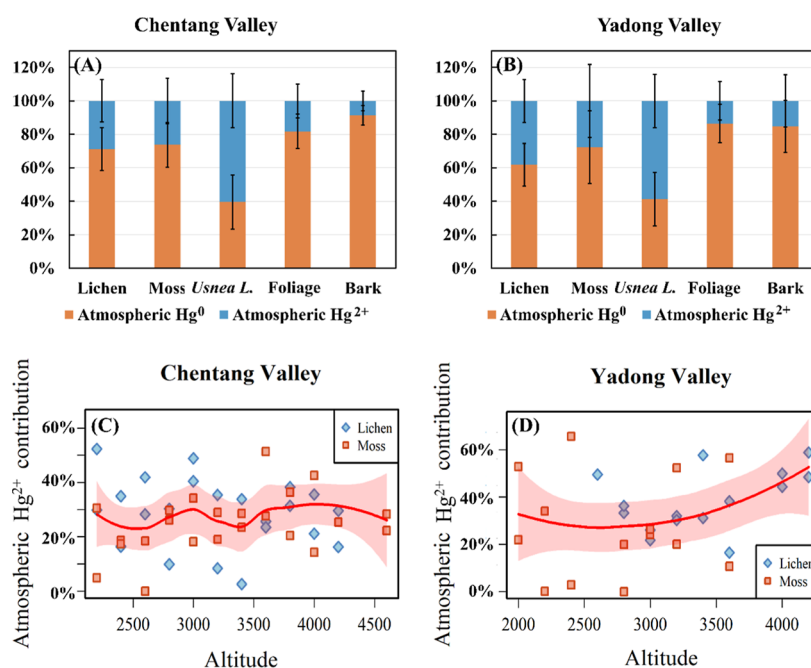


Figure 5. Source attribution estimated by the Hg isotopic mixing model in biomonitors for the (A) Chentang Valley and the (B) Yadong Valley. Variation of contribution of atmospheric Hg^{2+} sources in mosses and lichens of Chentang Valley (C) and Yadong Valley (D) along with the elevation. For data fitting, we used local polynomial regression and employed a five-fold cross-validation method to determine the smoothing parameter, and we added error bounds to illustrate the uncertainty of the fitted trend.

undergoes secondary reactions,^{33,38,51,81} causing a negative shift of $\sim 0.45\%$ $\Delta^{199}\text{Hg}$ in reactants.^{34,84} This is much lower than the $\Delta^{199}\text{Hg}$ shift of at least -0.8% required for *U. longissima* in Figure S6. Therefore, the Hg^0 re-emission processes cannot explain the highly negative $\Delta^{199}\text{Hg}$ values.

Likely, the aqueous secondary reactions of Hg^{2+} in the droplets on the surface of *U. longissima* contribute to the negative $\Delta^{199}\text{Hg}$ values. This is supported by several observations. The physiological traits and epiphytic environment of the *U. longissima*, coupled with an abundant dissolved organic matter (DOM) in precipitation and cloudwater, and deposited Hg^{2+} in two valleys (specifically at mid-altitude sites),^{60,69} facilitate aqueous Hg secondary reactions. The ~ 1.0 slope of $\Delta^{199}\text{Hg}$ to $\Delta^{201}\text{Hg}$ of *U. longissimas* in both valleys (Figure 4E,F) confirms the magnetic isotope effect induced by photochemical processes.^{33,84} Additionally, at mid-altitude sites of the Himalayas, changes from broadleaf forest to coniferous forest could result in elevated Hg deposition due to the increase of canopy biomass, thus influencing their chemical reactivities.⁸⁵ These changes can affect the magnitude the odd-MIF during photoreduction processes.^{86,87} This may explain the unusual negative $\Delta^{199}\text{Hg}$ values in *U. longissimas* at mid-altitude sites. We did not observe significant secondary reactions for lichens possibly for two reasons. One is that atmospheric Hg^0 is the main source. The other is that most lichens grow below the canopy with solar radiation shielding that weakens photo-reduction.

5. IMPLICATIONS

This study reveals Hg sources and accumulation mechanisms in biomonitors along with the elevation of the Himalayan valleys. We highlight that the rapid changes in climates, topography, and vegetation force a complicated Hg cycling, thus leading to the Hg concentration and isotopic signatures without altitudinal gradients in biomonitors. Specifically, the Hg secondary

reactions could lead to highly negative odd-MIF values in *U. longissima* at mid-altitude. Additionally, we determined that atmospheric Hg^0 was the main source of Hg in bark, foliage, mosses, and most lichens, but Hg in *U. longissimas* was mainly from atmospheric Hg^{2+} . Thus, using biomonitors to reflect the anthropogenic Hg transport in montane valleys has uncertainties because of the variability in Hg exchange at the interface between ambient air and biomonitors. On the other hand, the inconsistently altitudinal gradients likely reflect relatively weak transboundary transport of anthropogenic Hg across the Himalayan, although it is strong for POPs. Given Hg with a more complex biogeochemical cycling than POPs,^{19,88} the Hg cycling in the Himalayan valleys could mix the multiple impacts from montane environments and signals of transboundary transport of anthropogenic Hg from South Asia.

ASSOCIATED CONTENT

Supporting Information

The Supporting Information is available free of charge at <https://pubs.acs.org/doi/10.1021/acs.est.4c10224>.

Additional details for Monte Carlo simulation, regression analysis, and additional data for Hg signatures (PDF)

AUTHOR INFORMATION

Corresponding Author

Xun Wang – State Key Laboratory of Environmental Geochemistry, Institute of Geochemistry, Chinese Academy of Sciences, Guiyang 550081, China; orcid.org/0000-0002-7407-8965; Email: wangxun@mail.gyig.ac.cn

Authors

Xinyuan Cai – State Key Laboratory of Environmental Geochemistry, Institute of Geochemistry, Chinese Academy of Sciences, Guiyang 550081, China; University of Chinese Academy of Sciences, Beijing 100049, China

Wei Yuan – State Key Laboratory of Environmental Geochemistry, Institute of Geochemistry, Chinese Academy of Sciences, Guiyang 550081, China

Qiangong Zhang – Key Laboratory of Tibetan Environment Changes and Land Surface Processes, Institute of Tibetan Plateau Research, Chinese Academy of Sciences, Beijing 100101, China; orcid.org/0000-0002-2189-4248

Kang Luo – State Key Laboratory of Environmental Geochemistry, Institute of Geochemistry, Chinese Academy of Sciences, Guiyang 550081, China

Yiyuan Xu – State Key Laboratory of Environmental Geochemistry, Institute of Geochemistry, Chinese Academy of Sciences, Guiyang 550081, China

Ge Zhang – State Key Laboratory of Environmental Geochemistry, Institute of Geochemistry, Chinese Academy of Sciences, Guiyang 550081, China; College of Resources and Environmental Engineering, Guizhou University, Guiyang 550025, China

Fei Wu – State Key Laboratory of Environmental Geochemistry, Institute of Geochemistry, Chinese Academy of Sciences, Guiyang 550081, China

Longyu Jia – State Key Laboratory of Environmental Geochemistry, Institute of Geochemistry, Chinese Academy of Sciences, Guiyang 550081, China

Meiqing Sun – State Key Laboratory of Environmental Geochemistry, Institute of Geochemistry, Chinese Academy of Sciences, Guiyang 550081, China

Nantao Liu – State Key Laboratory of Environmental Geochemistry, Institute of Geochemistry, Chinese Academy of Sciences, Guiyang 550081, China

Che-Jen Lin – Center for Advances in Water and Air Quality, Lamar University, Beaumont, Texas 77710, United States

Xinbin Feng – State Key Laboratory of Environmental Geochemistry, Institute of Geochemistry, Chinese Academy of Sciences, Guiyang 550081, China; University of Chinese Academy of Sciences, Beijing 100049, China; orcid.org/0000-0002-7462-8998

Complete contact information is available at:
<https://pubs.acs.org/10.1021/acs.est.4c10224>

Notes

The authors declare no competing financial interest.

ACKNOWLEDGMENTS

This work was funded by the National Natural Science Foundation of China (42122053 and 42394093) and the Guizhou Provincial 2021 Science and Technology Subsidies (no. GZ2021SIG).

REFERENCES

- (1) Lindberg, S.; Bullock, R.; Ebinghaus, R.; Engstrom, D.; Feng, X.; Fitzgerald, W.; Pirrone, N.; Prestbo, E.; Seigneur, C. A Synthesis of Progress and Uncertainties in Attributing the Sources of Mercury in Deposition. *AMBIO* **2007**, *36* (1), 19–33.
- (2) Wang, X.; Yuan, W.; Lin, C.-J.; Luo, J.; Wang, F.; Feng, X.; Fu, X.; Liu, C. Underestimated Sink of Atmospheric Mercury in a Deglaciated Forest Chronosequence. *Environ. Sci. Technol.* **2020**, *54* (13), 8083–8093.
- (3) Selin, N. E.; Jacob, D. J.; Yantosca, R. M.; Strode, S.; Jaeglé, L.; Sunderland, E. M. Global 3-D land-ocean-atmosphere model for mercury: Present-day versus preindustrial cycles and anthropogenic enrichment factors for deposition. *Global Biogeochem. Cycles* **2008**, *22* (2), 2007GB003040.

- (4) Khalizov, A. F.; Viswanathan, B.; Larregaray, P.; Ariya, P. A. A Theoretical Study on the Reactions of Hg with Halogens: Atmospheric Implications. *J. Phys. Chem. A* **2003**, *107* (33), 6360–6365.

- (5) Qiu, J. China: The third pole. *Nature* **2008**, *454* (7203), 393–396.

- (6) Streets, D. G.; Horowitz, H. M.; Jacob, D. J.; Lu, Z.; Levin, L.; ter Schure, A. F. H.; Sunderland, E. M. Total Mercury Released to the Environment by Human Activities. *Environ. Sci. Technol.* **2017**, *51* (11), 5969–5977.

- (7) Yao, T.; Thompson, L. G.; Mosbrugger, V.; Zhang, F.; Ma, Y.; Luo, T.; Xu, B.; Yang, X.; Joswiak, D. R.; Wang, W.; et al. Third Pole Environment (TPE). *Environ. Develop.* **2012**, *3*, 52–64.

- (8) Kang, S.; Huang, J.; Wang, F.; Zhang, Q.; Zhang, Y.; Li, C.; Wang, L.; Chen, P.; Sharma, C. M.; Li, Q.; et al. Atmospheric Mercury Depositional Chronology Reconstructed from Lake Sediments and Ice Core in the Himalayas and Tibetan Plateau. *Environ. Sci. Technol.* **2016**, *50* (6), 2859–2869.

- (9) Huang, J.; Kang, S.; Feng, X.; Tang, W.; Ram, K.; Guo, J.; Zhang, Q.; Sharma, C. M.; Li, C.; Tripathee, L.; et al. Northward Extent of Atmospheric Mercury Transboundary Transport to the Himalayas and Tibetan Plateau Region. *Geophys. Res. Lett.* **2023**, *50* (4), No. e2022GL100948.

- (10) Huang, J.; Kang, S.; Tian, L.; Guo, J.; Zhang, Q.; Cong, Z.; Sillanpää, M.; Sun, S.; Tripathee, L. Influence of long-range transboundary transport on atmospheric water vapor mercury collected at the largest city of Tibet. *Sci. Total Environ.* **2016**, *566–567*, 1215–1222.

- (11) Huang, J.; Kang, S.; Yin, R.; Lin, M.; Guo, J.; Ram, K.; Li, C.; Sharma, C.; Tripathee, L.; Sun, S.; et al. Decoupling Natural and Anthropogenic Mercury and Lead Transport from South Asia to the Himalayas. *Environ. Sci. Technol.* **2020**, *54* (9), 5429–5436.

- (12) Yu, B.; Yang, L.; Liu, H.; Xiao, C.; Bu, D.; Zhang, Q.; Fu, J.; Zhang, Q.; Cong, Z.; Liang, Y.; et al. Tracing the Transboundary Transport of Mercury to the Tibetan Plateau Using Atmospheric Mercury Isotopes. *Environ. Sci. Technol.* **2022**, *56* (3), 1568–1577.

- (13) Yan, H.; Huang, J.; He, Y.; Liu, Y.; Wang, T.; Li, J. Atmospheric Water Vapor Budget and Its Long-Term Trend over the Tibetan Plateau. *J. Geophys. Res.:Atmos.* **2020**, *125* (23), No. e2020JD033297.

- (14) Ueno, K.; Toyotsu, K.; Bertolani, L.; Tartari, G. Stepwise Onset of Monsoon Weather Observed in the Nepal Himalaya. *Mon. Weather Rev.* **2008**, *136* (7), 2507–2522.

- (15) Lin, H.; Tong, Y.; Yin, X.; Zhang, Q.; Zhang, H.; Zhang, H.; Chen, L.; Kang, S.; Zhang, W.; Schauer, J.; et al. First measurement of atmospheric mercury species in Qomolangma Natural Nature Preserve, Tibetan Plateau, and evidence of transboundary pollutant invasion. *Atmos. Chem. Phys.* **2019**, *19* (2), 1373–1391.

- (16) Wang, X.; Zhang, Q.; Zhang, Y.; Cong, Z.; Xu, B.; Ji, Z.; Kang, S. The transboundary transport of air pollutants and their environmental impacts on Tibetan Plateau. *Chin. Sci. Bull.* **2019**, *64* (27), 2876–2884.

- (17) Bonasoni, P.; Laj, P.; Marinoni, A.; Sprenger, M.; Angelini, F.; Arduini, J.; Bonafé, U.; Calzolari, F.; Colombo, T.; Decesari, S.; et al. Atmospheric Brown Clouds in the Himalayas: first two years of continuous observations at the Nepal Climate Observatory-Pyramid (5079 m). *Atmos. Chem. Phys.* **2010**, *10* (15), 7515–7531.

- (18) Cong, Z.; Kang, S.; Gao, S.; Zhang, Y.; Li, Q.; Kawamura, K. Historical Trends of Atmospheric Black Carbon on Tibetan Plateau As Reconstructed from a 150-Year Lake Sediment Record. *Environ. Sci. Technol.* **2013**, *47* (6), 2579–2586.

- (19) Gong, P.; Wang, X.; Pokhrel, B.; Wang, H.; Liu, X.; Liu, X.; Wania, F. Trans-Himalayan Transport of Organochlorine Compounds: Three-Year Observations and Model-Based Flux Estimation. *Environ. Sci. Technol.* **2019**, *53* (12), 6773–6783.

- (20) Bargagli, R. Moss and lichen biomonitoring of atmospheric mercury: A review. *Sci. Total Environ.* **2016**, *572*, 216–231.

- (21) Garty, J. Biomonitoring Atmospheric Heavy Metals with Lichens: Theory and Application. *Crit. Rev. Plant Sci.* **2001**, *20* (4), 309–371.

- (22) Lodenius, M. Use of plants for biomonitoring of airborne mercury in contaminated areas. *Environ. Res.* **2013**, *125*, 113–123.

- (23) Klos, A.; Rajfur, M.; Sramek, I.; Waclawek, M. Mercury concentration in lichen, moss and soil samples collected from the forest areas of Praded and Glacensis Euroregions (Poland and Czech Republic). *Environ. Monit. Assess.* **2012**, *184* (11), 6765–6774.
- (24) Bargagli, R.; Monaci, F.; Bucci, C. Environmental biogeochemistry of mercury in Antarctic ecosystems. *Soil Biol. Biochem.* **2007**, *39* (1), 352–360.
- (25) Rimondi, V.; Costagliola, P.; Benesperi, R.; Benvenuti, M.; Beutel, M. W.; Buccianti, A.; Chiarantini, L.; Lattanzi, P.; Medas, D.; Parrini, P. Black pine (*Pinus nigra*) barks: A critical evaluation of some sampling and analysis parameters for mercury biomonitoring purposes. *Ecol. Indic.* **2020**, *112*, 106110.
- (26) Wang, X.; Yuan, W.; Lin, C.-J.; Feng, X. Mercury cycling and isotopic fractionation in global forests. *Crit. Rev. Environ. Sci. Technol.* **2022**, *52* (21), 3763–3786.
- (27) Yuan, W.; Wang, X.; Lin, C. J.; Wu, F.; Luo, K.; Zhang, H.; Lu, Z.; Feng, X. Mercury Uptake, Accumulation, and Translocation in Roots of Subtropical Forest: Implications of Global Mercury Budget. *Environ. Sci. Technol.* **2022**, *56* (19), 14154–14165.
- (28) Wang, X.; Yuan, W.; Lin, C.-J.; Feng, X. Mercury cycling and isotopic fractionation in global forests. *Crit. Rev. Environ. Sci. Technol.* **2022**, *52* (21), 3763–3786.
- (29) Dołęgowska, S.; Migaszewski, Z. M. Plant sampling uncertainty: a critical review based on moss studies. *Environ. Rev.* **2015**, *23* (2), 151–160.
- (30) Lodenius, M. Use of plants for biomonitoring of airborne mercury in contaminated areas. *Environ. Res.* **2013**, *125*, 113–123.
- (31) Chen, Y.; Xian, H.; Zhu, C.; Li, Y.; Pei, Z.; Yang, R.; Zhang, Q.; Jiang, G. The transport and distribution of novel brominated flame retardants (NBFRs) and organophosphate esters (OPEs) in soils and moss along mountain valleys in the Himalayas. *J. Hazard. Mater.* **2024**, *465*, 133044.
- (32) Yang, R.; Yao, T.; Xu, B.; Jiang, G.; Zheng, X. Distribution of organochlorine pesticides (OCPs) in conifer needles in the southeast Tibetan Plateau. *Environ. Pollut.* **2008**, *153* (1), 92–100.
- (33) Blum, J. D.; Sherman, L. S.; Johnson, M. W. Mercury Isotopes in Earth and Environmental Sciences. *Annu. Rev. Earth Planet. Sci.* **2014**, *42* (1), 249–269.
- (34) Demers, J. D.; Blum, J. D.; Zak, D. R. Mercury isotopes in a forested ecosystem: Implications for air-surface exchange dynamics and the global mercury cycle. *Global Biogeochem. Cycles* **2013**, *27* (1), 222–238.
- (35) Yin, R.; Feng, X.; Shi, W. Application of the stable-isotope system to the study of sources and fate of Hg in the environment: A review. *Appl. Geochem.* **2010**, *25* (10), 1467–1477.
- (36) Zheng, W.; Hintelmann, H. Mercury isotope fractionation during photoreduction in natural water is controlled by its Hg/DOC ratio. *Geochim. Cosmochim. Acta* **2009**, *73* (22), 6704–6715.
- (37) Zheng, W.; Obrist, D.; Weis, D.; Bergquist, B. A. Mercury isotope compositions across North American forests. *Global Biogeochem. Cycles* **2016**, *30* (10), 1475–1492.
- (38) Yuan, W.; Wang, X.; Lin, C.-J.; Wu, C.; Zhang, L.; Wang, B.; Sommar, J.; Lu, Z.; Feng, X. Stable Mercury Isotope Transition during Postdepositional Decomposition of Biomass in a Forest Ecosystem over Five Centuries. *Environ. Sci. Technol.* **2020**, *54* (14), 8739–8749.
- (39) Bergquist, B. A.; Blum, J. D. Mass-dependent and -independent fractionation of Hg isotopes by photoreduction in aquatic systems. *Science* **2007**, *318* (5849), 417–420.
- (40) Carignan, J.; Estrade, N.; Sonke, J. E.; Donard, O. F. X. Odd Isotope Deficits in Atmospheric Hg Measured in Lichens. *Environ. Sci. Technol.* **2009**, *43* (15), 5660–5664.
- (41) Chen, J.; Hintelmann, H.; Feng, X.; Dimock, B. Unusual fractionation of both odd and even mercury isotopes in precipitation from Peterborough, ON, Canada. *Geochim. Cosmochim. Acta* **2012**, *90*, 33–46.
- (42) Fu, X.; Jiskra, M.; Yang, X.; Maruszczak, N.; Enrico, M.; Chmieleff, J.; Heimbürger-Boavida, L. E.; Gheusi, F.; Sonke, J. E. Mass-Independent Fractionation of Even and Odd Mercury Isotopes during Atmospheric Mercury Redox Reactions. *Environ. Sci. Technol.* **2021**, *55* (14), 10164–10174.
- (43) Yuan, S.; Zhang, Y.; Chen, J.; Kang, S.; Zhang, J.; Feng, X.; Cai, H.; Wang, Z.; Wang, Z.; Huang, Q. Large Variation of Mercury Isotope Composition During a Single Precipitation Event at Lhasa City, Tibetan Plateau, China. *Procedia Earth Planet. Sci.* **2015**, *13*, 282–286.
- (44) Wang, Z.; Chen, J.; Feng, X.; Hintelmann, H.; Yuan, S.; Cai, H.; Huang, Q.; Wang, S.; Wang, F. Mass-dependent and mass-independent fractionation of mercury isotopes in precipitation from Guiyang, SW China. *C. R. Geosci.* **2015**, *347* (7–8), 358–367.
- (45) Rolison, J. M.; Landing, W. M.; Luke, W.; Cohen, M.; Salters, V. J. M. Isotopic composition of species-specific atmospheric Hg in a coastal environment. *Chem. Geol.* **2013**, *336*, 37–49.
- (46) Gratz, L. E.; Keeler, G. J.; Blum, J. D.; Sherman, L. S. Isotopic Composition and Fractionation of Mercury in Great Lakes Precipitation and Ambient Air. *Environ. Sci. Technol.* **2010**, *44* (20), 7764–7770.
- (47) Cai, H.; Chen, J. Mass-independent fractionation of even mercury isotopes. *Sci. Bull.* **2016**, *61* (2), 116–124.
- (48) Wang, X.; Lin, C. J.; Lu, Z.; Zhang, H.; Zhang, Y.; Feng, X. Enhanced accumulation and storage of mercury on subtropical evergreen forest floor: Implications on mercury budget in global forest ecosystems. *J. Geophys. Res.:Biogeosci.* **2016**, *121* (8), 2096–2109.
- (49) Yuan, W.; Wang, X.; Lin, C. J.; Zhang, H.; Feng, X.; Lu, Z. Impacts of Extreme Weather on Mercury Uptake and Storage in Subtropical Forest Ecosystems. *J. Geophys. Res.:Biogeosci.* **2022**, *127* (1), No. e2021JG006681.
- (50) Wang, X.; Luo, J.; Yuan, W.; Lin, C.-J.; Wang, F.; Liu, C.; Wang, G.; Feng, X. Global warming accelerates uptake of atmospheric mercury in regions experiencing glacier retreat. *Proc. Natl. Acad. Sci. U.S.A.* **2020**, *117* (4), 2049–2055.
- (51) Wang, X.; Luo, J.; Yin, R.; Yuan, W.; Lin, C.-J.; Sommar, J.; Feng, X.; Wang, H.; Lin, C. Using Mercury Isotopes To Understand Mercury Accumulation in the Montane Forest Floor of the Eastern Tibetan Plateau. *Environ. Sci. Technol.* **2017**, *51* (2), 801–809.
- (52) Wang, X.; Yuan, W.; Lin, C. J.; Wu, F.; Feng, X. Stable mercury isotopes stored in Masson Pinus tree rings as atmospheric mercury archives. *J. Hazard. Mater.* **2021**, *415*, 125678.
- (53) Blum, J. D.; Bergquist, B. A. Reporting of variations in the natural isotopic composition of mercury. *Anal. Bioanal. Chem.* **2007**, *388* (2), 353–359.
- (54) Estrade, N.; Carignan, J.; Sonke, J. E.; Donard, O. F. X. Measuring Hg Isotopes in Bio-Geo-Environmental Reference Materials. *Geostand. Geoanal. Res.* **2010**, *34* (1), 79–93.
- (55) Kang, H.; Liu, X.; Guo, J.; Wang, B.; Xu, G.; Wu, G.; Kang, S.; Huang, J. Characterization of mercury concentration from soils to needle and tree rings of Schrenk spruce (*Picea schrenkiana*) of the middle Tianshan Mountains, northwestern China. *Ecol. Indic.* **2019**, *104*, 24–31.
- (56) Wang, X.; Yuan, W.; Lin, C.-J.; Wu, F.; Feng, X. Stable mercury isotopes stored in Masson Pinus tree rings as atmospheric mercury archives. *J. Hazard. Mater.* **2021**, *415*, 125678.
- (57) Zhou, J.; Obrist, D.; Dastoor, A.; Jiskra, M.; Ryjkov, A. Vegetation uptake of mercury and impacts on global cycling. *Nat. Rev. Earth Environ.* **2021**, *2* (4), 269–284.
- (58) Stanković, J. D.; Sabovljević, A. D.; Sabovljević, M. S. Bryophytes and heavy metals: a review. *Acta Bot. Croat.* **2018**, *77* (2), 109–118.
- (59) Song, Z.; Sun, R.; Zhang, Y. Modeling mercury isotopic fractionation in the atmosphere. *Environ. Pollut.* **2022**, *307*, 119588.
- (60) Wang, X.; Yuan, W.; Lu, Z.; Lin, C. J.; Yin, R.; Li, F.; Feng, X. Effects of Precipitation on Mercury Accumulation on Subtropical Montane Forest Floor: Implications on Climate Forcing. *J. Geophys. Res.:Biogeosci.* **2019**, *124* (4), 959–972.
- (61) Bargagli, R. Atmospheric chemistry of mercury in Antarctica and the role of cryptogams to assess deposition patterns in coastal ice-free areas. *Chemosphere* **2016**, *163*, 202–208.
- (62) Onianwa, P. C. *Monitoring Atmospheric Metal Pollution: A Review of the Use of Mosses as Indicators*; Springer, 2001.

- (63) Bargagli, R.; Mikhailova, I. *Accumulation of Inorganic Contaminants. In Monitoring with Lichens—Monitoring Lichens*; Nimis, P. L., Scheidegger, C., Wolseley, P. A., Eds.; Springer Netherlands, 2002; pp 65–84.
- (64) Nieboer, E.; Richardson, D. H. S. The replacement of the nondescript term ‘heavy metals’ by a biologically and chemically significant classification of metal ions. *Environ. Pollut., Ser. B* **1980**, *1* (1), 3–26.
- (65) Enrico, M.; Roux, G. L.; Maruszcak, N.; Heimbürger, L. E.; Claustres, A.; Fu, X.; Sun, R.; Sonke, J. E. Atmospheric Mercury Transfer to Peat Bogs Dominated by Gaseous Elemental Mercury Dry Deposition. *Environ. Sci. Technol.* **2016**, *50* (5), 2405–2412.
- (66) Kinoshita, Y.; Hayase, S.; Yamamoto, Y.; Yoshimura, I.; Kurokawa, T.; Ahti, T.; Yamada, Y. Morphogenetic Capacity of the Mycobiont in Usnea. *Proc. Jpn. Acad., Ser. B* **1993**, *69*, 18–21.
- (67) Peng, F.; Bian, J.; Peng, P.; Reng, D.; Su, Y.; Sun, R. Research Progress of Genus Usnea. *Chem. Ind. For. Prod.* **2012**, *32* (1), 8.
- (68) Huang, J.; Kang, S.; Wang, L.; Liu, K.; Ram, K.; Sillanpää, M.; Tang, W.; Guo, J.; Zhang, Q.; Ma, M.; et al. Anthropogenic and natural drivers of seesaw-like spatial patterns in precipitation mercury over western China. *Environ. Pollut.* **2022**, *307*, 119525.
- (69) Blackwell, B. D.; Driscoll, C. T. Deposition of Mercury in Forests along a Montane Elevation Gradient. *Environ. Sci. Technol.* **2015**, *49* (9), 5363–5370.
- (70) Lawson, S. T.; Scherbatskoy, T. D.; Malcolm, E. G.; Keeler, G. J. Cloud water and throughfall deposition of mercury and trace elements in a high elevation spruce–fir forest at Mt. Mansfield, Vermont. *J. Environ. Monit.* **2003**, *5* (4), 578–583.
- (71) Bing, H.; Wu, Y.; Zhou, J.; Li, R.; Luo, J.; Yu, D. Vegetation and Cold Trapping Modulating Elevation-dependent Distribution of Trace Metals in Soils of a High Mountain in Eastern Tibetan Plateau. *Sci. Rep.* **2016**, *6* (1), 24081.
- (72) Zeng, S.; Wang, X.; Yuan, W.; Luo, J.; Wang, D. Mercury accumulation and dynamics in montane forests along an elevation gradient in Southwest China. *J. Environ. Sci.* **2022**, *119*, 1–10.
- (73) Chen, P.; Wang, X.; Yuan, W.; Wang, D. Typical heavy metals accumulation, transport and allocation in a deglaciated forest chronosequence, Qinghai-Tibet Plateau. *J. Hazard. Mater.* **2023**, *459*, 132162.
- (74) Arnold, J.; Gustin, M. S.; Weisberg, P. J. Evidence for Nonstomatal Uptake of Hg by Aspen and Translocation of Hg from Foliage to Tree Rings in Austrian Pine. *Environ. Sci. Technol.* **2018**, *52* (3), 1174–1182.
- (75) Gong, P.; Wang, X.; Xue, Y.; Zhang, L.; Wang, Y. Foliar uptake of persistent organic pollutants at alpine treeline. *J. Hazard. Mater.* **2023**, *453*, 131388.
- (76) Teixeira, D. C.; Lacerda, L. D.; Silva-Filho, E. V. Foliar mercury content from tropical trees and its correlation with physiological parameters in situ. *Environ. Pollut.* **2018**, *242*, 1050–1057.
- (77) Jiskra, M.; Sonke, J. E.; Obrist, D.; Bieser, J.; Ebinghaus, R.; Myhre, C. L.; Pfaffhuber, K. A.; Wangberg, I.; Kyllonen, K.; Worthy, D.; et al. A vegetation control on seasonal variations in global atmospheric mercury concentrations. *Nat. Geosci.* **2018**, *11* (4), 244–250.
- (78) Wang, X.; Chen, M.; Gong, P.; Wang, C. Perfluorinated alkyl substances in snow as an atmospheric tracer for tracking the interactions between westerly winds and the Indian Monsoon over western China. *Environ. Int.* **2019**, *124*, 294–301.
- (79) Slättberg, N.; Lai, H. W.; Chen, X.; Ma, Y.; Chen, D. Spatial and temporal patterns of planetary boundary layer height during 1979–2018 over the Tibetan Plateau using ERA5. *Int. J. Climatol.* **2022**, *42* (6), 3360–3377.
- (80) Guo, J.; Zhang, J.; Yang, K.; Liao, H.; Zhang, S.; Huang, K.; Lv, Y.; Shao, J.; Yu, T.; Tong, B.; et al. Investigation of near-global daytime boundary layer height using high-resolution radiosondes: first results and comparison with ERA5, MERRA-2, JRA-55, and NCEP-2 reanalyses. *Atmos. Chem. Phys.* **2021**, *21* (22), 17079–17097.
- (81) Liu, Y.; Liu, G.; Wang, Z.; Guo, Y.; Yin, Y.; Zhang, X.; Cai, Y.; Jiang, G. Understanding foliar accumulation of atmospheric Hg in terrestrial vegetation: Progress and challenges. *Crit. Rev. Environ. Sci. Technol.* **2022**, *52* (24), 4331–4352.
- (82) Vannini, A.; Nicolardi, V.; Bargagli, R.; Loppi, S. Estimating Atmospheric Mercury Concentrations with Lichens. *Environ. Sci. Technol.* **2014**, *48* (15), 8754–8759.
- (83) Stankwitz, C.; Kaste, J. M.; Friedland, A. J. Threshold increases in soil lead and mercury from tropospheric deposition across an elevational gradient. *Environ. Sci. Technol.* **2012**, *46* (15), 8061–8068.
- (84) Zheng, W.; Hintelmann, H. Isotope Fractionation of Mercury during Its Photochemical Reduction by Low-Molecular-Weight Organic Compounds. *J. Phys. Chem. A* **2010**, *114* (12), 4246–4253.
- (85) Ma, Y.; Shang, L.; Hu, H.; Zhang, W.; Chen, L.; Zhou, Z.; Singh, P. B.; Hu, Y. Mercury distribution in the East Himalayas: Elevational patterns in soils and non-volatile small mammals. *Environ. Pollut.* **2021**, *288*, 117752.
- (86) Haitzer, M.; Aiken, G. R.; Ryan, J. N. Binding of mercury(II) to dissolved organic matter: The role of the mercury-to-DOM concentration ratio. *Environ. Sci. Technol.* **2002**, *36* (16), 3564–3570.
- (87) Gu, B.; Bian, Y.; Miller, C. L.; Dong, W.; Jiang, X.; Liang, L. Mercury reduction and complexation by natural organic matter in anoxic environments. *Proc. Natl. Acad. Sci. U.S.A.* **2011**, *108*, 1479–1483.
- (88) Beckers, F.; Rinklebe, J. Cycling of mercury in the environment: Sources, fate, and human health implications: A review. *Crit. Rev. Environ. Sci. Technol.* **2017**, *47* (9), 693–794.